American Mineralogist, Volume 92, pages 761–770, 2007

Deriving formation constants for aqueous metal complexes from XANES spectra: Zn^{2+} and Fe^{2+} chloride complexes in hypersaline solutions

Weihua Liu,[1,2,*] Barbara Etschmann,[1] Garry Foran,[3] Michael Shelley,[4] and Joël Brugger[2,5]

[1]CSIRO Exploration and Mining, School of Geosciences, Monash University, Clayton, Victoria 3800, Australia
[2]South Australian Museum, North Terrace, Adelaide, South Australia 5000, Australia
[3]Australian National Beamline Facility, Photon Factory, KEK, Oho 1-1, Tsukuba-shi, Ibaraki-ken 305-0801, Japan
[4]Research School of Earth Science, Australian National University, ACT 0200, Australia
[5]School of Earth and Environmental Sciences, University of Adelaide, Adelaide, South Australia 5005, Australia

Abstract

The development of numerical modeling of reactive transport relies on the availability of thermodynamic properties for the solid, surface, aqueous, and vapor species stable at the conditions of interest. The lack of experimental studies and comprehensive activity-composition models severely limits the predictive capabilities of these models in systems involving highly saline fluids or low-density volatile-rich fluids. X-ray absorption near-edge structure spectroscopy (XANES) is a powerful technique to study the speciation of transition metals in aqueous fluids: it is element specific; sensitive to the oxidation state of the metal, the ligand field and the coordination geometry of the complex; and it is suitable for measuring trace amounts of metals (<1 wt%) in solutions over a wide pressure and temperature range.

Formation constants for the aqueous complexes of transition metals can be determined from a series of XANES spectra obtained on solutions containing a constant amount of the metal of interest and variable concentrations of a ligand. The method relies on a non-linear, least-squares-fitting approach, with full distribution of species calculations based on a complete thermodynamic model for the experimental system under consideration. The technique is particularly suitable for following octahedral to tetrahedral transitions among weak chloride complexes of transition metals. The log K for the reaction $Zn^{2+}_{(octahedral)} + 4Cl^- = ZnCl^{2-}_{4\,(tetrahedral)}$ at 25 °C is retrieved to be 0.1(6), within error of the accepted literature value. The same method applied to Fe^{2+}-chloride complexes shows that the log K for the reaction $Fe^{2+}_{(octahedral)} + 4Cl^- = FeCl^{2-}_{4\,(tetrahedral)}$ increases from –6.2(6) at 25 °C to –2.9(3) at 150 °C. This study confirms that tetrahedral chloride complexes play an important role in Fe transport in hypersaline brines especially at elevated temperatures, and shows that XANES is well suited to study systems that may be difficult to study with other techniques.

Keywords: Fe and Zn chloride complexes, XAS, XANES, stability constants, thermodynamics, hydrothermal solutions

Introduction

Speciation of metals in aqueous solution

Reactive-transport modeling is a powerful tool for understanding and predicting the distribution of elements in the Earth's crust. Applications vary from contaminant transport around waste deposits, to the formation of ore deposits, to high-temperature corrosion in power plants (e.g., Heinrich et al. 1996; van der Lee and De Windt 2001). Reactive-transport modeling requires an understanding of the nature of all aqueous complexes, surface species, minerals, melts and gases present, and relies on the accuracy of thermodynamic models accounting for activity-composition relationships over the P, T, and composition range of interest (e.g., Anderson and Crerar 1993; Bethke 1996). Yet, speciation and activity-composition relationships are still poorly understood under some important conditions, including highly concentrated brines and low-density volatile-rich hydrothermal fluids. The improvement of the scope and accuracy of reactive-transport modeling relies on the development of experimental techniques suitable to obtain quantitative information on mineral solubility and aqueous speciation over a wide range of conditions (P, T, composition).

Conventionally most thermodynamic properties for aqueous metal complexes at elevated temperatures have been derived from mineral solubility measurements, with some from UV-Vis and potentiometric measurements. The past decade has seen dramatic improvements in the spectroscopic techniques available for studying aqueous speciation and solubility. Among these, X-ray absorption spectroscopy (XAS) appears particularly suitable, because it allows concurrent studies of mineral solubility and speciation quantitatively in-situ to high pressure and temperature (e.g., Pokrovski et al. 2005; Testemale et al. 2005). The technique can provide direct information on the nature, number, and distances of the nearest neighbors around a metal center or around a ligand such as Br^- (e.g., Seward et al. 1999; Simonet

* E-mail: weihua.liu@csiro.au

et al. 2002). The technique has also been used to study metal speciation in natural fluid inclusions to high temperature (e.g., Anderson et al. 1998; Mavrogenes et al. 2002).

The use of the two main XAS techniques, X-ray absorption near-edge structure (XANES) and extended X-ray absorption fine structure (EXAFS), for quantitative studies of element speciation in complex samples such as soils is well established (e.g., Isaure et al. 2002), but few studies have used these techniques to retrieve quantitative thermodynamic properties for aqueous complexes. A pioneering study of Inada and Funahashi (1999) showed that it was possible to measure the formation constant for ferric $FeCl^{2+}$ complex from EXAFS data at room temperature. The advantages of XAS are multiple: (1) the coordination structure and thermodynamic properties can be determined from the same experimental data; (2) the high brightness of third generation synchrotron sources makes XAS suitable for measurements on dilute systems (metal concentrations <1 wt%) through thick windows, enabling in situ spectroscopy at high *P-T* (e.g., Fulton et al. 2001; Testemale et al. 2005); (3) XANES is particularly sensitive to coordination changes in aqueous complexes, which effect a first-order control on the solubility of many metals in saline brines at room temperature and at elevated *P-T* (e.g., Susak and Crerar 1985); (4) in comparison with UV-Vis-NIR spectrophotometry, XAS is not affected by deviations from the Beer-Lambert law related to the change in the refractive index of solvent, which may affect the accuracy of UV-Vis studies of metal speciation in concentrated electrolytes (e.g., Vinokurov and Kankare 1998); and (5) XAS is element specific, hence interference from other constituents of the experimental system are limited.

Zn^{2+} chloride complexes

Chloride complexes of $Zn^{2+}$are the main species responsible for the transport of Zn in hydrothermal systems, and the stability of Zn^{2+} chloride complexes has been studied experimentally over conditions ranging from room temperature to supercritical aqueous solutions (e.g., Ruaya and Seward 1986; Bourcier and Barnes 1987; Barrett and Anderson 1988; Cygan et al. 1994; Uchida et al. 1998; Wesolowski et al. 1998). There is good agreement for the room-temperature speciation (Fig. 1a), however, there still appears to be some controversy regarding the geometry and stoichiometry of Zn^{2+} chlorides at elevated *T*. Experimental studies (generally limited to salinity <1 *m*; Ruaya and Seward's (1986) to 3.5 *m* Cl_{tot}) suggest that the neutral octahedral $ZnCl_{2(aq)}$ is the most stable form of Zn in hydrothermal fluids at $T \geq 400$ °C, but studies from natural fluid inclusions show that tetrahedral $ZnCl_4^{2-}$ is the dominant species in hypersaline brines up to 430 °C (Anderson et al. 1995, 1998). This result was also confirmed qualitatively by Mayanovic et al. (1999), who showed that $ZnCl_4^{2-}$ was predominant at up to 660 °C in solutions containing 8 *m* Cl.

The speciation of Zn^{2+} at room temperature is dominated by octahedral Zn^{2+} and tetrahedral $ZnCl_4^{2-}$, with low-order Zn^{2+} chlorides existing only in small proportion (<30 mol%; Fig. 1a). This makes retrieving properties for these intermediate species particularly difficult.

Fe^{2+} chloride complexes

Ferrous iron is very mobile in near-surface environments, and is the most stable aqueous form of Fe in crustal fluids. Fe^{2+} chloride complexes are widely acknowledged to be predominant in many hydrothermal fluids; however, the nature and thermodynamic properties of Fe^{2+}-chloride complexes in hypersaline brines are still poorly understood, and there is no consensus about the speciation of Fe^{2+} in brines. There have been a few

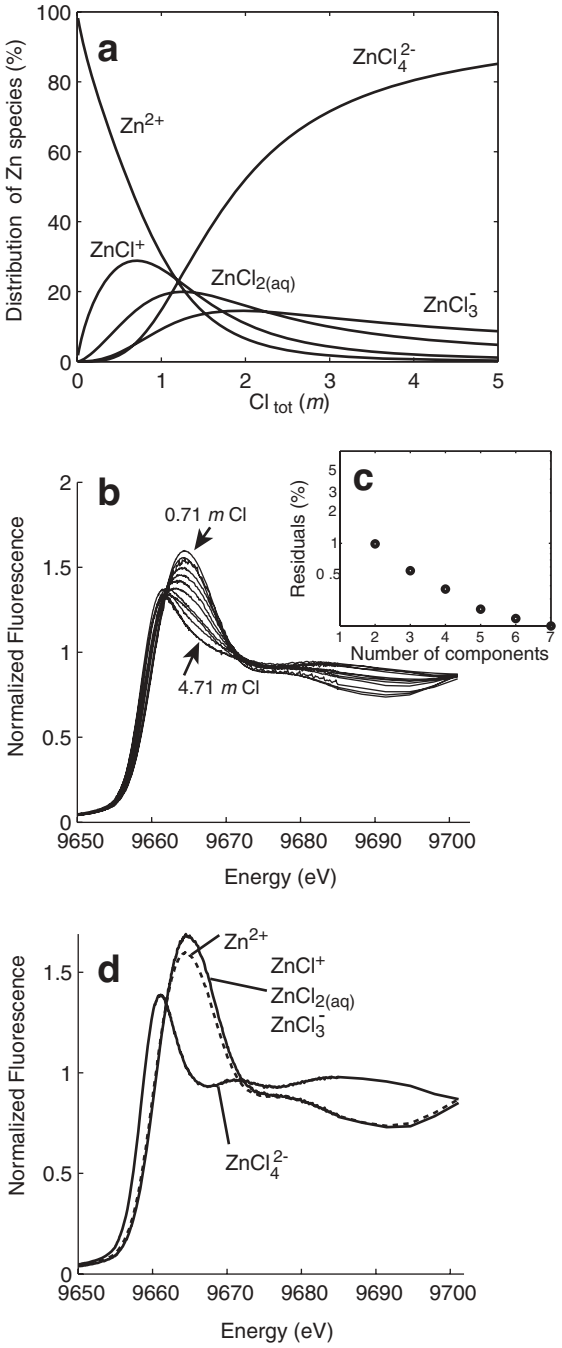

Figure 1. XANES study of Zn^{2+} chloride complexes at 25 °C. (**a**) Distribution of species for Zn^{2+} in acidic NaCl solution, using thermodynamic properties from Ruaya and Seward (1986). (**b**) XANES spectra of solutions (compositions listed in Table 1) with varying NaCl concentrations. (**c**) Principal Component Analysis for data in **b**. Two components explain 99% of the variance. (**d**) Extracted spectra for the individual species.

experimental studies to investigate the stability of Fe^{2+} chloride complexes at elevated temperatures and pressures, including solubility measurements (Chou and Eugster 1977; Crerar et al. 1978; Boctor et al. 1980; Wood et al. 1987; Ding and Seyfried 1992; Fein et al. 1992; Ohmoto et al. 1994), potentiometric studies (Palmer and Hyde 1993), and UV-Vis spectrophotometric studies (Po and Sutin 1968; Koplitz et al. 1987; Heinrich and Seward 1990; Zhao and Pan 2001). Most of the solubility studies suggest that $FeCl^+$ and $FeCl_{2(aq)}$ are the dominant species in solution, which is supported by the potentiometric measurements of Palmer and Hyde (1993) and the UV-Vis study of Heinrich and Seward (1990). However, the chloride concentrations used in these studies were too low (<3 *m*) to allow for unambiguous detection of the higher-order chloride complexes presumably present in hypersaline brines. In contrast, two UV-Vis-NIR spectrophotometric studies (Koplitz et al. 1987; Zhao and Pan 2001) conducted using chloride concentrations up to 16 *m* suggest that the tetrahedral $FeCl_4^{2-}$ complex becomes important with increasing temperature or increasing chloride concentration.

Many studies have used Fe *K*-edge XAS to determine the oxidation state and speciation of Fe in compounds, minerals, and glasses (e.g., Waychunas et al. 1983; Bajt et al. 1994; Westre et al. 1997; Dyar et al. 1998; Galoisy et al. 2001; Wilke et al. 2001; Isaure et al. 2002; Berry et al. 2003; O'Day et al. 2004). In contrast, comparatively few studies have used XANES and EXAFS to investigate Fe^{2+} complexes in hydrothermal solutions, and in particular Fe^{2+} chloride complexes. Apted et al. (1985) conducted EXAFS measurement for aqueous Fe^{3+} and Fe^{2+} chloride complexes, but they were not able to observe the existence of tetrahedral Fe^{2+} chloride complexes as their experiments were limited to room temperature and chloride concentrations of 4 and 8 *m*.

Fe-*K* XANES is particularly sensitive to the oxidation state and coordination geometry of Fe in dilute samples (<1 wt% Fe). Typically, Fe *K*-edge XANES spectra display a small pre-edge peak attributed to the $1s \rightarrow 3d$ electronic transition, a shoulder to the edge attributed to the $1s \rightarrow 4s$ transition, and the edge crest due to the $1s \rightarrow 4p$ transition (Waychunas et al. 1983; Berry et al. 2003) (Fig. 2). Octahedral Fe^{2+} complexes show a low-intensity $1s \rightarrow 3d$ transition, because the electric dipole transition is forbidden in the centro-symmetric octahedral coordination, and the weak intensity is due to quadrupole coupling effects. In contrast, this transition has a high probability in non-centro-symmetric tetrahedrally coordinated Fe^{2+} compounds (Waychunas et al. 1983; Westre et al. 1997; Galoisy et al. 2001). The inset in Figure 2 illustrates this effect for the minerals siderite ($FeCO_3$; Fe in octahedral coordination with 6 O atoms) and hercynite ($FeAl_2O_4$; Fe in tetrahedral coordination with 4 O atoms). The edge and after-edge features also reflect the differences of the two coordination structures.

This paper aims to show how XAS—specifically XANES—can be used to retrieve equilibrium constants for the formation of aqueous complexes. The method is illustrated using a series of XANES spectra of acidic aqueous solutions containing ~1 wt% Zn^{2+} or Fe^{2+} and different concentrations of chloride introduced as NaCl or LiCl. This paper also reports the first value for the formation constant for the tetrahedral $FeCl_4^{2-}$ complex measured at elevated temperature (150 °C).

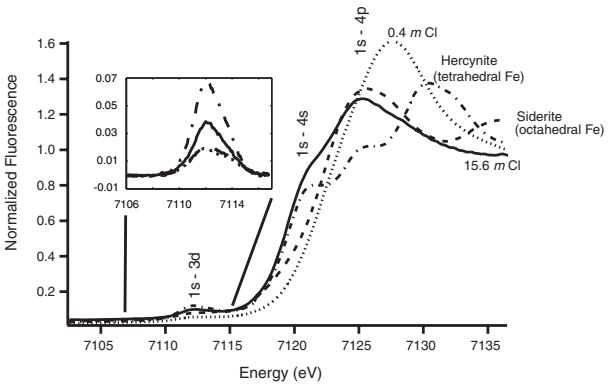

FIGURE 2. XANES spectra of siderite ($FeCO_3$), hercynite ($FeAl_2O_4$), 0.4 *m* and 15.6 *m* total chloride solutions at 150 °C. The pre-edge range is shown in the insert.

EXPERIMENTAL SETUP

Sample preparation

Analytical grade Zn^{2+} chloride ($ZnCl_2$), Fe^{2+} chloride tetrahydrate ($FeCl_2 \cdot 4H_2O$), lithium chloride (LiCl), and sodium chloride (NaCl) were purchased from Sigma Aldrich and used without further treatment. All solutions were prepared using doubly deionized water, to which 0.1 *m* hydrochloric acid was added to prevent hydrolysis. For Fe^{2+}, the water was boiled and flushed with nitrogen gas, then introduced into a glove box filled with nitrogen gas. Inside the glove box, the acid and salts were added and the solution was loaded into the spectroscopic cell. The amount of Fe^{3+} in the sample solutions is considered negligible (<0.5%), as determined by examining UV-Vis spectra of solutions prepared in an identical manner. UV-Vis spectrophotometry is very sensitive to even trace amounts of Fe^{3+}, as the molar absorptivity of Fe^{3+} chloride complexes is up to 1000 times higher than that of Fe^{2+} chloride complexes (e.g., Heinrich and Seward 1990). The compositions of the sample solutions are listed in Tables 1 (Zn) and 2 (Fe). XANES spectra of two minerals containing Fe^{2+} in octahedral (siderite, Fe_2CO_3) and tetrahedral (hercynite, $FeAl_2O_4$) coordination were also measured. The solid samples were crushed and diluted with boron nitride to around 1% by weight prior to measurement.

TABLE 1. Composition of Zn-bearing NaCl solutions used for Zn *K*-edge XANES measurements

Sample no.	Cl_{tot} (*m*)	Na_{tot} (*m*)	Zn_{tot} (*m*)
1	0.716	0.000	0.308
2	1.203	0.485	0.309
3	1.667	0.967	0.300
4	2.013	1.303	0.305
5	2.201	1.481	0.310
6	2.477	1.749	0.314
7	2.671	1.965	0.303
8	2.976	2.260	0.308
9	3.215	2.503	0.306
10	3.705	2.993	0.306
11	4.387	3.669	0.309
12	4.715	3.995	0.310

TABLE 2. Composition of Fe-bearing LiCl solutions used for Fe *K*-edge XANES measurements

Sample no.	Cl_{tot} (*m*)	Li_{tot} (*m*)	Fe_{tot} (*m*)
1	0.392	0.00	0.146
2	3.39	3.00	0.145
3	4.956	4.53	0.163
4	6.242	5.85	0.146
5	7.542	7.04	0.201
6	8.43	7.97	0.180
7	9.646	9.12	0.213
8*	10.438	10.06	0.139
9	11.29	10.73	0.230
10*	12.038	11.55	0.194
11	13.082	12.45	0.266
12	15.614	15.04	0.237

* Not used in 150 °C data fitting.

Experimental cell

The cell used for measuring the solutions is built from grade 2 titanium, with a 100 µm thick Kapton film as an X-ray window (Fig. 3). The cylindrical titanium cell body has an internal volume of approximately 0.5 cm^3, and is heated by an aluminum block with two cartridge heaters (Fig. 3a). The cell body and heater were enclosed in a ceramic insulator to reduce heat loss (Fig. 3b). The temperature is controlled by a solid-state relay unit and is measured using two type-K thermocouples located near the level of the X-ray windows.

XANES measurement and preparation

Iron (7112 eV) and Zn (9659 eV) *K*-edge XANES spectra of the ions dissolved in acidic chloride solutions containing up to 15 *m* LiCl (Fe) and 4 *m* NaCl (Zn) were measured at 25 °C (Fe, Zn) and 150 °C (Fe) using beamline BL-20B (Australian National Beamline Facility, ANBF) at the Photon Factory, Japan. BL-20B is a bending magnet beam line equipped with a water-cooled channel cut Si (111) monochromator with 1.87 eV energy bandpass of the monochromator at Fe *K*-edge. Combined with the Fe*K*α core-hole width of 1.25 eV, this results in an energy resolution of 2.2 eV for Fe-*K* edge. Zinc has a core-hole width of 1.94 eV at the *K*α edge resulting in an energy resolution of 3.6 eV. The ring was operating in uniform-bunch mode with a beam size of 2.5 × 0.5 mm (Fe edge) and in single-bunch mode with a beam size of 3.0 × 0.2 mm (Zn edge). The incident beam intensity I_0 was measured with an ionization chamber using a N_2 fill gas at atmospheric pressure. Data were measured in fluorescence mode with a Canberra GL0110S 10 element array Ge solid-state detector and collected from 7094 to 7292 eV, using 0.25 eV steps from 7094 to 7109 eV; 0.1 eV steps from 7109 to 7117 eV; 0.25 eV steps from 7117 to 7137 eV; and 2.5 eV steps from 7137 to 7292 eV. Similarly, the Zn data were collected from 9640 to 10 200 eV, using 0.125 eV steps from 9640 to 9655; 0.05 eV steps from 9655 to 9665 eV; 0.125 eV step from 9665 to 9685; and 3.2 eV steps from 9685 to 10 200 eV. The Fe and Zn edge energies were calibrated using a Fe or Zn foil, respectively.

Self-absorption effects were assessed using the Fluo code (Haskel 1999). This correction increased the amplitude of the white line by up to 14% (Zn) and 7% (Fe) of the normalized edge-height. We ran the data analysis on both corrected and uncorrected spectra, but found that the values of the thermodynamic properties retrieved using the raw or corrected data were well within the quoted 90% confidence level error (see below). Consequently, we show only the raw data in the figures.

XANES spectra were background-corrected and normalized using the AUTOBK program (Newville et al. 1993). For the Fe-*K* edge data, the pre-edge region of the XANES spectrum was extracted using an inverse tangent function coupled with a linear background to model the edge jump. In this procedure, the pre-edge peak was modeled using pseudo-Voigt curves. Although theoretical predictions show that there are three electronic transitions for octahedral Fe^{2+} complexes and four transitions for tetrahedral complexes (Westre et al. 1997; Galoisy et al. 2001), it was found that the pre-edge peak in all spectra could be modeled using two pseudo-Voigt peaks: one at 7112 eV and another at 7114 eV (Fig. 4). The inclusion of more Voigt peaks did not decrease the residuals. Wilke et al. (2001) similarly found that only two peaks are required to fit the pre-edge feature of 4-coordinated Fe^{2+} minerals. This is probably a result of the relatively poor resolution of the experiment (2.2 eV for our data).

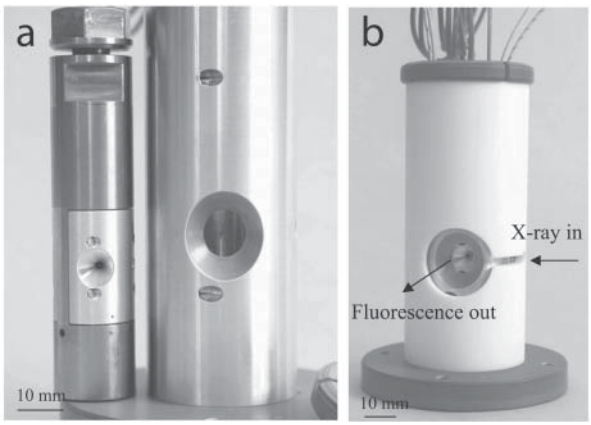

Figure 3. Hydrothermal cell with Kapton windows used for XAS measurements at elevated temperature. (**a**, left) Titanium cell, with the X-ray out window at the front; (**a**, right) aluminum block containing the cartridge heaters and thermocouple shafts. (**b**) Cell in working condition, with ceramic insulator mounted. The beam path for fluorescence experiments is indicated.

Data interpretation

XAS data can be interpreted using the Beer-Lambert law (e.g., Chantler et al. 2000, 2001), and this forms the basis of our quantitative interpretation to retrieve thermodynamic properties. The Beer-Lambert law relates the observed total molar absorption (A_λ) at a certain wavelength (λ) to the molarity (M_i) and molar absorptivity of individual species ($\varepsilon_{i,\lambda}$). For a transmission experiment, assuming that absorbance by the solvent is identical for all solutions, the Beer-Lambert law can be written as:

$$A_\lambda = l\sum_{i=1}^{n} M_i \varepsilon_{i,\lambda} \quad (1a)$$

where l is the path length of the sample cell in centimeters. For fluorescence XANES data, the spectra are normalized to a unit step height. In this case the Beer-Lambert law can be written as:

$$\tilde{A}_\lambda = l\sum_{i=1}^{n} x_i \tilde{\varepsilon}_{i,\lambda} \quad (1b)$$

where $\tilde{A}_\lambda$ is the normalized fluorescence at wavelength λ, $\tilde{\varepsilon}_{i,\lambda}$ is the normalized individual spectrum of the i^{th} contributing species, and x_i is the fraction of the i^{th} species contributing to the XANES spectrum. In our case the contributing species are the metal chloride complexes XCl_i^{2-i}, X = Fe or Zn, with i = 0 to 4, and the mole fraction x_i is expressed as:

$$x_i = \frac{M_{XCl_i^{2-i}}}{\sum_i M_{XCl_i^{2-i}}} = \frac{m_{XCl_i^{2-i}}}{\sum_i m_{XCl_i^{2-i}}} \quad (1c)$$

Note that concentrations in Equation 1c can be expressed either in molarity (M) or molality (m)—we use the molality scale throughout this paper.

Brugger et al. (2007) developed an algorithm to derive thermodynamic properties of aqueous complexes from UV-Vis-NIR data for metal complexes based on the Beer-Lambert law. This approach has been applied to UV-Vis experiments of aqueous Cu^{2+} chloride (Brugger et al. 2001), Cu(I) chloride (Liu et al. 2001), and Fe^{3+} chloride complexes (Liu et al. 2006). The data interpretation used here is similar to the previous works, so only a brief introduction is given.

The thermodynamic model

The following aqueous species are included in the model: H^+, Li^+, Na^+, Cl^-, $LiCl_{(aq)}$, $NaCl_{(aq)}$, $HCl_{(aq)}$, X^{2+}, and four X^{2+} chloride complexes (X = Fe, Zn). Hydroxide species are not included in the model as under the acidic conditions (0.1 *m* HCl) used in these experiments, little deprotonation of water coordinated to X^{2+} is expected [pKa1 for $Fe(H_2O)_6^{2+}$ is 9.31 at 25 °C and 6.63 at 150 °C; pKa1 for $Zn(H_2O)_6^{2+}$ is 7.84 at 25 °C (Shock et al. 1997)]. The concentrations and activities of aqueous species were calculated by solving simultaneously the following mass action, mass balance, and charge balance equations:

$$K_{HCl_{(aq)}} = \frac{m_{HCl_{(aq)}} \overline{\gamma}_{HCl_{(aq)}}}{m_{H^+} m_{Cl^-} \overline{\gamma}_{H^+} \overline{\gamma}_{Cl^-}} \quad (2)$$

$$K_{LiCl_{(aq)}} = \frac{m_{LiCl_{(aq)}} \overline{\gamma}_{LiCl_{(aq)}}}{m_{Li^+} m_{Cl^-} \overline{\gamma}_{Li^+} \overline{\gamma}_{Cl^-}} \text{ or } K_{NaCl_{(aq)}} = \frac{m_{NaCl_{(aq)}} \overline{\gamma}_{NaCl_{(aq)}}}{m_{Na^+} m_{Cl^-} \overline{\gamma}_{Na^+} \overline{\gamma}_{Cl^-}} \quad (3)$$

$$K_{XCl_i^{2-i}} = \frac{m_{MCl_i^{2-i}} \overline{\gamma}_{MCl_i^{2-i}}}{m_{X^{2+}} \overline{\gamma}_{X^{2+}} (m_{Cl^-} \overline{\gamma}_{Cl^-})^i}, (i = 1 \text{ to } 4) \quad (4)$$

$$m_{X_{total}} = \sum_i m_{XCl_i^{2-i}}, \text{(Fe mass balance)} \quad (5)$$

$$m_{Cl_{total}} = m_{HCl_{(aq)}} + m_{LiCl_{(aq)}} + m_{Cl^-} + \sum_i i m_{XCl_i^{2-i}}, \text{(Cl mass balance)} \quad (6)$$

$$m_{Li_{total}} = m_{LiCl_{(aq)}} + m_{Li^+}, \text{ or } m_{Na_{total}} = m_{NaCl_{(aq)}} + m_{Na^+}, \text{(Na or Li mass balance)} \quad (7)$$

$$m_{H^+} + m_{Li^+} + m_{Na^+} + \sum_i (2-i) m_{XCl_i^{2-i}} = m_{Cl^-}, \text{(Charge balance)} \quad (8)$$

$$x_i = \frac{m_{XCl_i^{2-i}}}{\sum_i m_{XCl_i^{2-i}}} \text{ (for Eq. 1b)} \quad (9)$$

where K, m, and γ refer to the formation constant, molal concentration, and activity coefficient for the subscripted individual species, respectively, and i in Equations 2–9 refers to the number of chloride ligands.

A model enabling calculation of activity coefficients to high ionic strength is needed to solve the above equations and calculate thermodynamic formation constants for X^{2+} chloride complexes. Unfortunately traditional activity coefficient models based on the Debye-Hückel equations (e.g., B-dot equation, Helgeson 1969) are only valid in dilute solutions. Here we follow the empirical method suggested by Brugger et al. (2001), which extends the B-dot equation of Helgeson (1969) to high salinity (up to 18 m LiCl) by adding a quadratic term. This approach allows us to describe accurately the experimental mean molal stoichiometric activity coefficient data for LiCl and NaCl solutions (i.e., Holmes and Mesmer 1983), and yields internally consistent activity coefficients for the X^{2+} chloride complexes. The main advantage of this method is that at low salinity (≤ 2 m), it is identical to the extended Debye-Hückel formalism used in most studies of metal transport and deposition under hydrothermal conditions. Note that the formation constants obtained for species stable at high salinity should be treated as apparent only, as their values depend upon the choice of the activity model. The following extended form of the Debye-Hückel equation was used:

$$\log(\overline{\gamma}_n) = -\frac{A_\gamma Z_n^2 \overline{I}^{1/2}}{1 + B_\gamma \mathring{a}_n \overline{I}^{1/2}} + b_{\gamma,SALT} \overline{I} + b_{\gamma_{sq},SALT} \overline{I}^2 + \Gamma_\gamma \quad (10)$$

where A_γ and B_γ are the Debye-Hückel solvent parameters taken from Helgeson and Kirkham (1974), and $b_{\gamma,SALT}$ is the extended-term parameter (b-dot coefficient) for LiCl or NaCl dominated solutions, $\mathring{a}_n$ is the distance of closest approach of ion n, and is given a value of 5 Å for divalent and trivalent ions, and 4.0 Å for monovalent ions, except for H^+ and Fe^{2+}, which are given a value of 9 and 6 Å, respectively (Kielland 1937). $\overline{I}$ is the effective ionic strength using the molal scale. Γ_γ is a mole fraction to molality conversion factor and $b_{\gamma_{sq},SALT}$ is a quadratic term added to the Debye-Hückel equation to extend its validity to high chloride concentrations. The activity coefficient of the neutral species $NaCl_{(aq)}$, $LiCl_{(aq)}$, $FeCl_{2(aq)}$, and $ZnCl_{2(aq)}$ was estimated with the Setchénow equation (see Brugger et al. 2001):

$$\log\left[\overline{\gamma}_{LiCl_{(aq)}}\right] = b_{\gamma,LiCl_{(aq)}} \overline{I} + \Gamma_\gamma \quad (11)$$

For LiCl solutions, values of the b-dot coefficient ($b_{\gamma,LiCl}$), Setchénow coefficient [$b_{\gamma,LiCl_{(aq)}}$] and the extended quadratic coefficient ($b_{\gamma_{sq},LiCl}$), at each experimental temperature were taken from Brugger et al. (2001). For NaCl solutions, fitting to the mean stoichiometric activity coefficients values from Oelkers and Helgeson (1991) yields the following values: $b_{\gamma_{sq},NaCl(25°C)} = -0.000299$ and $b_{\gamma,NaCl_{(aq)}} = 0.317$, while the value for $b_{\gamma,NaCl}$ was taken from Helgeson and Kirkham (1974). Setchénow coefficients for $ZnCl_{2(aq)}$ and $FeCl_{2(aq)}$ are set to 0.1, as in Brugger et al. (2001). Dissociation constants for $NaCl_{(aq)}$, $LiCl_{(aq)}$, and $HCl_{(aq)}$ were taken from the SUPCRT database (Johnson et al. 1992) (Table 3). Dissociation constants for $FeCl^+$ and $FeCl_{2(aq)}$ are from a polynomial fitting of log K values of Zhao and Pan (2001), and for $ZnCl^+$, $ZnCl_{2(aq)}$, and $ZnCl_3^-$ from Ruaya and Seward (1986) (Table 3). The activity coefficient for $HCl_{(aq)}$ was assumed to be unity, as accurate pH estimates are not required.

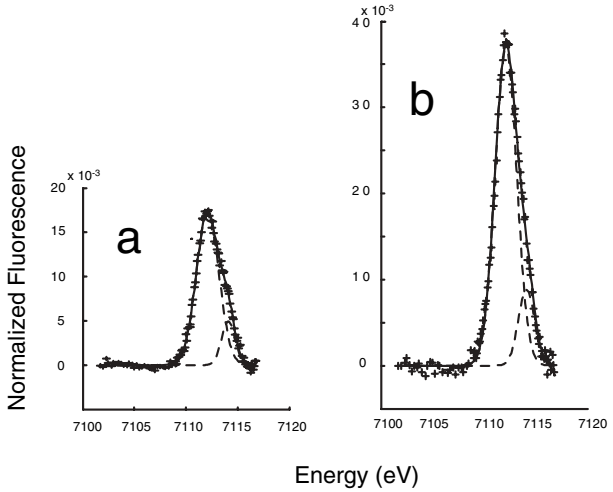

FIGURE 4. Deconvoluted spectra of the Fe pre-edge peak for the Fe^{2+}-bearing 0.4 m Cl solution (**a**), and 15.6 m Cl solution (**b**) at 150 °C. Crosses represent measured data and solid lines stand for the fitted values using two Voigt peaks that are shown as dashed lines.

TABLE 3. Dissociation constants for aqueous species included in the speciation calculation

	25 °C	150 °C	Data sources
$HCl_{(aq)}$	0.71	0.52	Johnson et al. 1992
$LiCl_{(aq)}$	1.51	0.88	Johnson et al. 1992
$NaCl_{(aq)}$	0.78	0.21	Johnson et al. 1992
$ZnCl^+$	–0.42	–2.86	Ruaya and Seward 1986
$ZnCl_{2(aq)}$	–0.62	–2.91	Ruaya and Seward 1986
$ZnCl_3^-$	–0.34	–2.10	Ruaya and Seward 1986
$FeCl^+$	0.37	–0.86	Zhao and Pan 2001*
$FeCl_{2(aq)}$	1.74	0.03	Zhao and Pan 2001*

* Polynomial fitting results of the data from Zhao and Pan (2001) of 10–100 °C.

Error analysis

The uncertainties in the fitted log *K* values can come from the following three sources: (1) experimental errors related to sample preparation and data collection, together with uncertainty resulting from colinearity between the concentration profiles and spectra of the contributing species; (2) uncertainty in the calculation of the activity coefficients; and (3) uncertainty in the speciation model, in particular the values of the stability constants for the reactions that are not refined. For example, the uncertainties for the formation constants for $FeCl^+$ and $FeCl_2$(aq) quoted in Zhao and Pan (2001) range from 0.02 to 0.16 log units, which will also affect the uncertainties in the fitted log *K* values for $FeCl_4^{2-}$. The choice of the parameters used in the activity coefficient model (Eq. 10), particularly the ion size parameter $å_n$, will also result in errors in the fitted log *K* values, as discussed in Liu et al. (2002). It is difficult to quantify accurately the total errors in the fitted log *K* values, as they are not the linear sum of the uncertainties from different sources. Here we have chosen to report only the uncertainty related to (1), neglecting the model-specific error sources (2) and (3). The errors are obtained by examining the values of the residuals as a function of the value for the optimized log *K* values, as in previous studies (Brugger 2006; Brugger et al. 2001; Liu et al. 2001, 2002). This also allows determination of the nature of the minimum (global vs. local) and identification of possible alternative local minima. The residual *R* in percentage is defined as the difference between the observed values (y_i) and the calculated values (y):

$$R = 100\sqrt{\frac{\sum(y_i - y)^2}{\sum y_i^2}} \quad (12)$$

The range of uncertainties in the optimized log *K* values are then estimated based on the residual maps at 90% confidence level using the nonlinear-regression calculation method of Draper and Smith (1998).

Fitting results

Zn^{2+} chlorides at 25 °C

The XANES spectra of Zn^{2+} in chloride solutions are shown in Figure 1b. With increasing salt concentration, the intensity of the edge crest decreases and shifts toward lower energy. Two nearly isosbestic points are observed at 9662 and 9672 eV, indicating that only two major components with distinct spectra in the solutions contribute to the observed spectra. Principal component analysis (PCA; Fig. 1c) also shows that two factors are sufficient to explain the spectra with 99% accuracy. The fitting procedure in this case is made especially difficult by the strong underdetermination of the problem, resulting from the fact that: (1) five species are probably present, but statistically the data displays only two linearly independent components; (2) three species occur only in minor proportion (Fig. 1a); and (3) the octahedral species (Zn^{2+}, $ZnCl^+$, $ZnCl_{2(aq)}$, and $ZnCl_3^-$) are likely to have very similar spectra. To circumvent these difficulties, we applied the following constraints during the fitting: (1) the log *K* of all species except $ZnCl_4^{2-}$ were fixed to the literature values; (2) the spectrum of Zn^{2+} was fixed to be equal to the spectrum of the solution containing the least amount of chloride (solution 1, Table 1); (3) the spectra of all three "octahedral" Zn^{2+}-chloride complexes were constrained to be equal. During the fit, the spectra of the octahedral Zn^{2+}-chloride complexes and that of $ZnCl_4^{2-}$ were optimized together with the log *K* for $ZnCl_4^{2-}$. A similar approach was also applied to the fit of Fe^{2+} chloride systems. The optimized spectra shown in Figure 1d confirm that the octahedral species (Zn^{2+} to $ZnCl_3^-$) have similar spectra. The log *K* for $ZnCl_4^{2-}$ retrieved using the above procedure is 0.1(6) using the data corrected for self-absorption), very close to the 0.19 value from Ruaya and Seward (1986). Based on the residual map, the uncertainty in the derived log *K* for $ZnCl_4^{2-}$ is ±0.6.

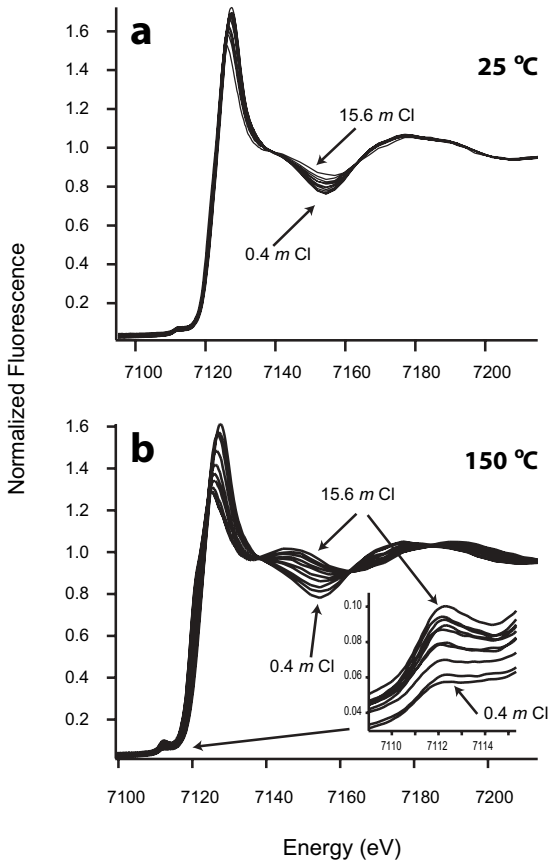

Figure 5. Fe *K*-edge XANES spectra of Fe^{2+} bearing LiCl solutions at 25 °C (**a**) and 150 °C (**b**). The pre-edge range of 150 °C data is shown in the insert.

Fe^{2+} chlorides at 25 and 150 °C

The normalized Fe *K*-edge XANES spectra for Fe-bearing LiCl solutions are shown in Figure 5a for 25 °C and Figure 5b for 150 °C. The 150 °C data show a more pronounced change with increasing Cl concentration, compared to the 25 °C data. The pre-edge peak is centered at ~7112 eV, and its intensity increases with increasing chloride concentration; this is accompanied by a shift in the edge position toward lower energy and a decrease of edge intensity (Figs. 5 and 6). In the after-edge region we can also see a systematic change in the spectra: with increasing chloride concentration, the intensity of the band at 7140–7160 eV

increases and that of the band between 7170–7180 eV decreases (Figs. 5 and 6).

Three isosbestic points are observed at energies of 7138, 7162, and 7185 eV for the 150 °C data (Fig. 5b), indicating that only two major components with distinct spectra in the solutions contribute to the observed spectra. The isosbestic points for the 25 °C data are less obvious (Fig. 5a).

The normalized Fe *K*-edge XANES spectra of the two end-member solutions with chloride concentrations of 0.4 and 15.6 *m* are shown in Figure 2 together with minerals containing Fe^{2+} in octahedral and tetrahedral coordination. The XANES spectra of siderite and the 0.4 *m* Cl solution show a broad main edge peak, with an edge crest of 7121 eV for siderite and 7126 eV for the 0.4 *m* Cl solution. The XANES spectra of tetrahedral Fe in hercynite shows $1s \rightarrow 3d$ transitions at 7112 eV, and $1s \rightarrow 4p$ transitions at 7121.5 and 7125.5 eV. These two features can also be seen in the 15.6 *m* Cl solution, but the 7130 eV peak of hercynite is absent in the spectrum obtained from the 15.6 *m* Cl solution. The extracted pre-edge spectrum (insert in Fig. 2) clearly shows that the pre-edge feature of the $1s \rightarrow 3d$ transition is stronger for hercynite and the 15.6 *m* chloride solution, compared to siderite and the 0.4 *m* chloride solution, as expected for tetrahedral and octahedral geometry, respectively. Therefore, the systematic change of the pre-edge, together with the features of the edge, qualitatively reveal the change of structure of Fe^{2+} chloride complexes from octahedral to tetrahedral coordination with increasing chloride concentration at a given temperature. The two absorbing species responsible for the observed isosbestic points are thus interpreted as octahedral and tetrahedral Fe^{2+} chloride complexes.

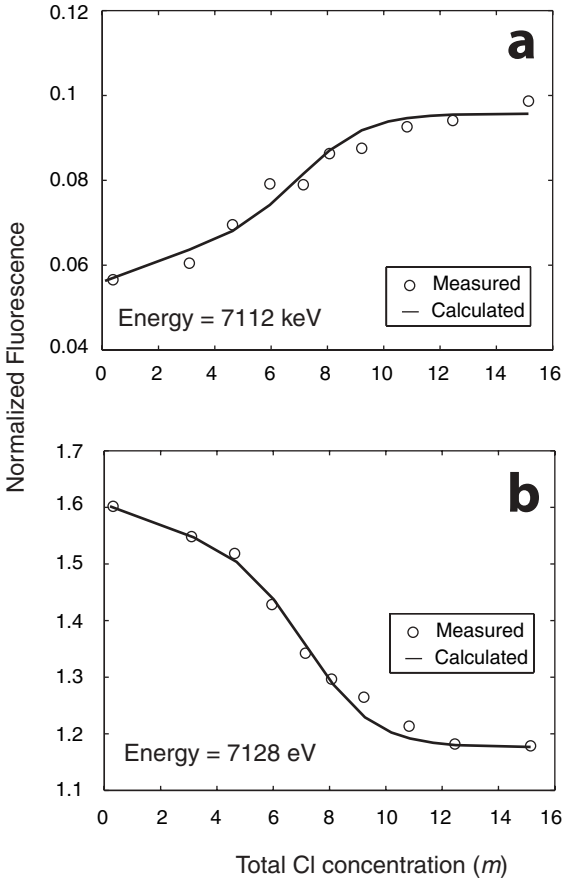

FIGURE 6. Normalized X-ray fluorescence at a fixed energy as a function of chloride concentrations at 150 °C, (**a**) at 7112 eV and (**b**) at 7128 eV. The circles show the measured absorption and the lines represent fitted values using log *K* values generated from this study.

Previous studies showed that three Fe^{2+} chloride complexes may exist in aqueous chloride solutions: octahedral $FeCl^+$ and $FeCl_{2(aq)}$, and tetrahedral $FeCl_4^{2-}$. Based on UV-Vis spectroscopic data, Heinrich and Seward (1990) identified $FeCl^+$ and $FeCl_{2(aq)}$ in solutions containing up to 3 *m* Cl at temperatures up to 200 °C. They observed that $FeCl_{2(aq)}$ becomes more important with increasing temperature. This result was subsequently supported by the solubility experiments of Fein et al. (1992), Ding and Seyfried (1992), and Ohmoto et al. (1994), and by the potentiometric measurements of Palmer and Hyde (1993). However, the UV-Vis studies of Koplitz et al. (1987) and Zhao and Pan (2001) found $FeCl_4^{2-}$ in concentrated LiCl solutions with Cl concentrations up to 15 *m*. Zhao and Pan (2001) also estimated thermodynamic properties for $FeCl_4^{2-}$ at 60, 80, and 90 °C. Therefore Fe^{2+}, $FeCl^+$, $FeCl_{2(aq)}$, and $FeCl_4^{2-}$ are included in the speciation model. As the changes in the XANES spectra are mainly attributed to the change of coordination from octahedral to tetrahedral, and the formation constants of the octahedral $FeCl^+$ and $FeCl_{2(aq)}$ are well-known, only the formation constant (log *K*) for the tetrahedral species ($FeCl_4^{2-}$) is optimized in the fitting (Eq. 13):

$$Fe^{2+} + 4Cl^- = FeCl_4^{2-} \quad (13)$$

and the log *K* values for $FeCl^+$ and $FeCl_{2(aq)}$ were fixed to those determined by Zhao and Pan (2001). Alternative fitting procedures including optimization of $FeCl_3^-$ were tested, but resulted in unrealistic spectra; therefore this species is not included in the fitting. This is consistent with the speciation model of Zhao and Pan (2001), in which they also found no evidence for $FeCl_3^-$.

Three different data sets constructed from different parts of the XAS spectra were fitted to derive log *K* values for $FeCl_4^{2-}$ at 150 °C. Data set A is the normalized XANES spectra including pre-edge and after-edge range, data set B contains only the pre-edge range, and data set C includes pre-edge spectra that are weighted by a factor of 10, plus the after-edge range. The fitting results are compiled in Table 4. It is encouraging that all three data sets give very similar log *K* values, which indicates that the octahedral to tetrahedral transition is well reflected by both pre-edge and after-edge spectra. The log *K* value (–2.92) fitted

TABLE 4. Fitted logarithm of formation constants (log *K*) for $FeCl_4^{2-}$ from Fe *K*-edge XANES spectra of Fe^{2+}-bearing LiCl solutions at 25 and 150 °C

Temperature	Data set	Energy range (eV)	Fitted log *K* for $FeCl_4^{2-}$
150 °C	A: pre-edge + after-edge	7102–7220	–2.92 ± 0.3 –2.90 ± 0.3*
	B: pre-edge only	7102–7117	–3.05 ± 0.4
	C: after-edge + 10 X pre-edge	7102–7220	–2.99 ± 0.3
25 °C	Pre-edge + after-edge	7102–7220	–6.22 ± 0.6 –6.27 ± 0.6*

* Using self-absorption corrected spectra.

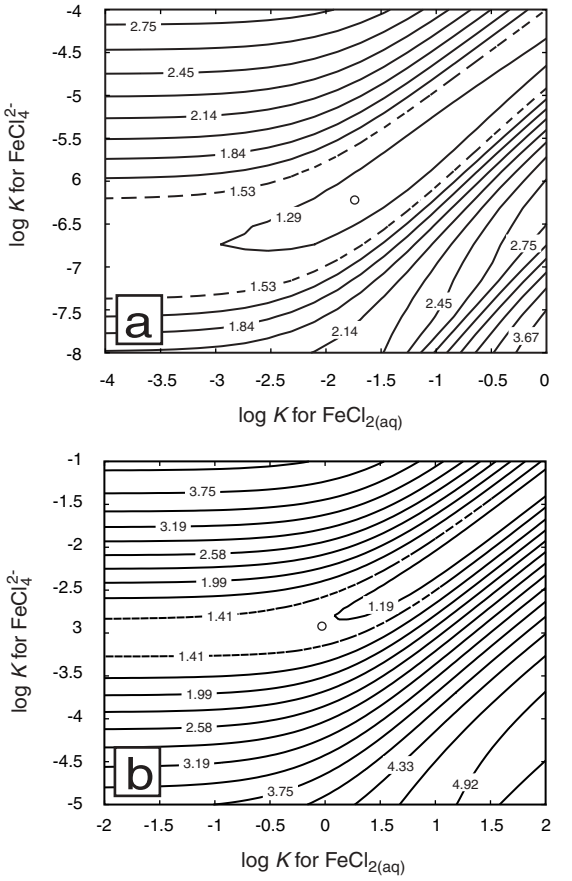

FIGURE 7. Calculated residuals as a function of log K values for $FeCl_{2(aq)}$ and $FeCl_4^{2-}$ at 25 and 150 °C. The circles represent the location of fitted log K values. An approximate 90% confidence region is defined by the dashed contours (1.53% at 25 °C and 1.41 at 150 °C, respectively).

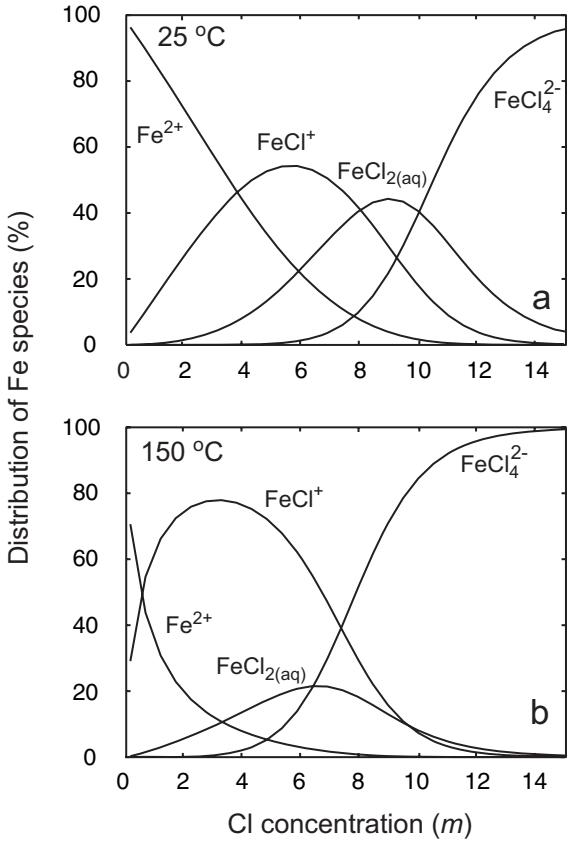

FIGURE 8. Fe^{2+} speciation in acidic LiCl solutions at 25 °C and 150 °C calculated using log K values for $FeCl_4^{2-}$ generated from this study.

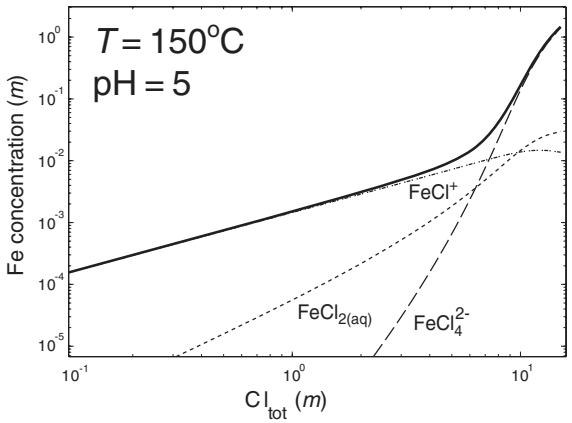

FIGURE 9. Solubility of magnetite (Fe_3O_4) in chloride solutions at 150 °C under reducing condition [$a_{H_{2(aq)}} = 10^{-5}$] at a fixed pH of 5. Solid lines represent total Fe concentration, and the dashed lines refer to the concentrations of individual Fe^{2+} chloride complexes indicated in the figure.

from the total spectra (data set A) was chosen as final result. As the pre-edge peak for 25 °C data is less intense, the whole spectra (7102–7220 eV) were included in the fitting. Given that the self-absorption correction increased the amplitude of the white line, the log K values were determined for these spectra. The difference in fitted log K values between uncorrected and corrected data are less than 0.15 log unit (Table 4), well below the estimated errors (0.3–0.6, Table 4).

Although a few studies have qualitatively revealed the existence of the $FeCl_4^{2-}$ complex (Susak and Crerar 1985; Koplitz et al. 1987), only one study (Zhao and Pan 2001) reported the formation constants for $FeCl_4^{2-}$ at 60, 80, and 90 °C (log K of –4.1, –3.45, and –2.96 at the respective temperatures). Our values for log K are –6.2(6) at 25 °C and –2.9(3) at 150 °C, slightly lower than the extrapolation of their values. Note that the values of Zhao and Pan (2001) are considered as the first-order approximation, as their log K values are based on the slope of $FeCl_4^{2-}$ concentration vs. Fe and Cl concentration and the assumption that the activity coefficient terms cancel out (Zhao and Pan 2001).

Figure 7 shows the residual mapped as a function of log $K_{FeCl_4^{2-}}$ and log $K_{FeCl_{2(aq)}}$ at 25 °C (Fig. 7a) and 150 °C (Fig. 7b). It can be seen that the log $K_{FeCl_4^{2-}}$ and log $K_{FeCl_{2(aq)}}$ are correlated, which means values and uncertainties of log $K_{FeCl_4^{2-}}$ depends on the choice of log $K_{FeCl_{2(aq)}}$ used in the calculation. The reported uncertainties in fitted log K values (Table 4) are derived from the extent of the confidence region defined by the contour at 1.3 times the absolute minimum (1.53% at 25 °C and 1.41% at 150 °C, Fig. 7), corresponding approximately to the 90% confidence

level using the nonlinear-regression calculation method of Draper and Smith (1998).

Figure 8 shows the calculated speciation of Fe^{2+} chloride complexes based on our new log K values for $FeCl_4^{2-}$ at 25 and 150 °C. It can be seen from the figure that the predominance field of $FeCl_4^{2-}$ shifts from 10 m LiCl at 25 °C to 7 m at 150 °C. It is expected that at temperatures above 150 °C, the predominance field of the $FeCl_4^{2-}$ complex extends to even lower chloride concentrations, which agrees with the trend that the tetrahedral complexes of transition metals become important with increasing temperature and/or chloride concentrations, as described by previous studies (e.g., Susak and Crerar 1985; Koplitz et al. 1987; Zhao and Pan 2001).

Discussions and concluding remarks

This study demonstrates that XANES spectra can be used to derive formation constants for aqueous transition-metal complexes in a way analogous to UV-Vis-NIR spectrophotometry. XANES is particularly well suited for systems in which the metal of interest displays changes in coordination geometry. This, however, also indicates the limitation of this method. When there is no change in coordination, the change observable in the XANES spectra may be small, and it may not be possible to derive log K values. As shown in the Fe^{2+} and Zn^{2+} systems, the successive replacement of water by chloride ligands in an octahedral complex has little effect on the XANES spectra, and all octahedral chloride complexes show similar XANES spectra. Therefore, it was impossible to derive formation constants for these species, and it was necessary to use the properties derived from other techniques in the analysis of the XANES data. This means that XANES is particularly powerful as a complement of the methods that are not sensitive to coordination changes, e.g., solubility or potentiometric studies. Note that EXAFS data can be treated in the same way as XANES, and are more sensitive to stepwise ligand substitution (e.g., Inada and Funahashi 1999); this will become increasingly attractive as "fast EXAFS" techniques, which allow the collection of many spectra within a reasonable time frame, become more routine.

The present study confirms the increasing stability of tetrahedral species relative to octahedral species with increasing salt concentration and increasing temperature for Fe^{2+} and Zn^{2+}; the significance of such a trend was first noticed for transition-metals chloride complexes by Susak and Crerar (1985) using UV-Vis measurements. Such coordination changes mark steep gradients in solubility curves (e.g., Fig. 9), indicating that dilution or cooling may result in efficient precipitation of the metals as the octahedral complex replaces a high-order tetrahedral complex (Fig. 9).

The possibility to conduct XAS experiments at elevated pressure and temperature (e.g., Bassett et al. 2000; Fulton et al. 2001; Testemale et al. 2005) opens new opportunities for the study of metal transport and deposition under conditions typical of magmatic-hydrothermal ore-forming environments (>500 °C, ≥1 kbar). The XANES spectra can further be complemented by EXAFS spectra, to increase the amount of information both for speciation and thermodynamic analyses. XANES appears to be well suited to track coordination changes among transition metals quantitatively under magmatic hydrothermal conditions.

Acknowledgments

The authors thank James Hester for assisting with the experiments at the Photon Factory. This study was supported by the Australian Synchrotron Research Program (Grant to W.L. and B.E., Fellowship to B.E.) and by the Australian Research Council (Fellowship DP0208323 to J.B.). The authors also thank D. Cole, G. Pokrovski, and an anonymous reviewer for their helpful comments.

References cited

Anderson, A.J., Mayanovic, R.A., and Bajt, S. (1995) Determination of the local structure and speciation of zinc in individual hypersaline fluid inclusions by micro-XAFS. Canadian Mineralogist, 33, 499–508.

——— (1998) A microbeam XAFS study of aqueous chlorozinc complexing to 430 °C in fluid inclusions from the Knaum granitic pegmatite, Saxonian granulite facies, Germany. Canadian Mineralogist, 36, 511–524.

Anderson, G.M. and Crerar, D.A. (1993) Thermodynamics in Geochemistry, 588 p. Oxford University Press, New York.

Apted, M.J., Waychunas, G.A., and Brown, G.E. (1985) Structure and specification of iron complexes in aqueous solutions determined by X-ray absorption spectroscopy. Geochimica et Cosmochimica Acta, 49, 2081–2089.

Bajt, S., Sutton, S.R., and Delaney, J.S. (1994) X-Ray microprobe analysis of iron oxidation-states in silicates and oxides using X-ray-absorption near-edge structure (XANES). Geochimica et Cosmochimica Acta, 58, 5209–5214.

Barrett, T.J. and Anderson, G.M. (1988) The solubility of sphalerite and galena in 1–5 m NaCl solutions to 300 °C. Geochimica et Cosmochimica Acta, 52, 813–820.

Bassett, W.A., Anderson, A.J., Mayanovic, R.A., and Chou, I.M. (2000) Hydrothermal diamond anvil cell for XAFS studies of first-row transition elements in aqueous solution up to supercritical conditions. Chemical Geology, 167, 3–10.

Berry, A.J., O'Neill, H.S., Jayasuriya, K.D., Campbell, S.J., and Foran, G.J. (2003) XANES calibrations for the oxidation state of iron in a silicate glass. American Mineralogist, 88, 967–977.

Bethke, C.M. (1996) Geochemical reaction modeling, concepts and applications, 397 p. Oxford University Press, New York.

Boctor, N.Z., Popp, R.K., and Frantz, J.D. (1980) Mineral-solution equilibria—IV. Solubilities and the thermodynamic properties of $FeCl^{\circ}_2$ in the system Fe_2O_3-H_2-H_2O-HCl. Geochimica et Cosmochimica Acta, 44, 1509–1518.

Bourcier, W.L. and Barnes, H.L. (1987) Ore Solution Chemistry—VII. Stabilities of chloride and bisulfide complexes of zinc to 350 °C. Economic Geology, 82, 1839–1863.

Brugger, J. (2006) BeerOz, a suite of MATLAB routines for the quantitative thermodynamic interpretation of electronic spectra of aqueous complexes. Computers in Geosciences, 33, 248–261.

Brugger, J., McPhail, D.C., Black, J., and Spiccia, L. (2001) Complexation of metal ions in brines: application of electronic spectroscopy in the study of the Cu^{2+}-LiCl-H_2O system between 25 and 90 °C. Geochimica et Cosmochimica Acta, 65, 2691–2708.

Chantler, C.T. (2000) Detailed Tabulation of Atomic Form Factors, Photoelectric Absorption and Scattering Cross Section, and Mass Attenuation Coefficients in the Vicinity of Absorption Edges in the Soft X-ray (Z = 30–36, Z = 60–89, E = 0.1 keV–10 keV), Addressing Convergence Issues of Earlier Work. Journal of Physical and Chemical Reference Data, 29, 597.

Chantler, C.T., Tran, C.Q., Paterson, D., Cookson, D., and Barnea, Z. (2001) X-ray extended-range technique for precision measurement of the X-ray mass attenuation coefficient and Im(f) for copper using synchrotron radiation. Physics Letters A, 286, 338–346.

Chou, I.M. and Eugster, H.P. (1977) Solubility of magnetite in supercritical chloride solutions. American Journal of Science, 277, 1296–1314.

Crerar, D.A., Susak, N.J., Borcsik, M., and Schwartz, S. (1978) Solubility of the buffer assemblage pyrite + pyrrhotite + magnetite in NaCl solutions from 200 to 350 °C. Geochimica et Cosmochimica Acta, 42, 1427–1438.

Cygan, G.L., Hemley, J.J., and D'Angelo, W.M. (1994) An experimental study of zinc chloride speciation from 300 to 600 °C and 0.5 to 2.0 kbar in buffered hydrothermal solutions. Geochimica et Cosmochimica Acta, 58, 4841–4855.

Ding, K. and Seyfried, W.E., Jr. (1992) Determination of iron-chlorine complexing in the low-pressure supercritical region (sodium chloride fluid): Iron solubility constraints on pH subseafloor hydrothermal fluids. Geochimica et Cosmochimica Acta, 56, 3681–3692.

Draper, N.R. and Smith, H. (1998) Applied regression analysis, 706 p. Wiley-Interscience, New York.

Dyar, M.D., Delaney, J.S., Sutton, S.R., and Schaefer, M.W. (1998) Fe^{3+} distribution in oxidized olivine: A synchrotron micro-XANES study. American Mineralogist, 83, 1361–1365.

Fein, J.B., Hemley, J.J., D'Angelo, W.M., Komninou, A., and Sverjensky, D.A. (1992) Experimental study of iron-chloride complexing in hydrothermal fluids. Geochimica et Cosmochimica Acta, 56, 3179–3190.

Fulton, J.L., Darab, J.G., and Hoffmann, M.M. (2001) X-ray absorption spectroscopy and imaging of heterogeneous hydrothermal mixtures using a diamond

microreactor cell. Review of Scientific Instruments, 72, 2117–2122.
Galoisy, L., Calas, G., and Arrio, M.A. (2001) High-resolution XANES spectra of iron in minerals and glasses: structural information from the pre-edge region. Chemical Geology, 174, 307–319.
Haskel, D. (1999) Fluo: Correcting XANES for self-absorption in fluorescence measurements, http://www.aps.anl.gov/xfd/people/haskel/fluo.html.
Heinrich, C.A. and Seward, T.M. (1990) A spectrophotometric study of aqueous iron(II) chloride complexing from 25 to 200 °C. Geochimica et Cosmochimica Acta, 54, 2207–2221.
Heinrich, C.A., Walshe, J.L., and Harrold, B.P. (1996) Chemical mass transfer modelling of ore-forming hydrothermal systems—current practice and problems. Ore Geology Reviews, 10, 319–338.
Helgeson, H.C. (1969) Thermodynamics of hydrothermal systems at elevated temperatures and pressures. American Journal of Science, 267, 729–804.
Helgeson, H.C. and Kirkham, D.H. (1974) Theoretical prediction of the thermodynamic behavior of aqueous electrolytes at high pressures and temperatures; II, Debye-Huckel parameters for activity coefficients and relative partial molal properties. American Journal of Science, 274, 1199–1261.
Holmes, H.F. and Mesmer, R.E. (1983) Thermodynamic properties of aqueous solutions of the alkali metal chlorides to 250 °C. Journal of Physical Chemistry, 87, 1242–1255.
Inada, Y. and Funahashi, S. (1999) Equilibrium and structural study of chloro complexes of iron(III) ion in acidic aqueous solution by means of X-ray absorption spectroscopy. Zeitschrift Fur Naturforschung Section B—a Journal of Chemical Sciences, 54, 1517–1523.
Isaure, M.P., Laboudigue, A., Manceau, A., Sarret, G., Tiffreau, C., Trocellier, P., Lamble, G., Hazemann, J.L., and Chateigner, D. (2002) Quantitative Zn speciation in a contaminated dredged sediment by μ-PIXE, μ-SXRF, EXAFS spectroscopy and principal component analysis. Geochimica et Cosmochimica Acta, 66, 1549–1567.
Johnson, J.W., Oelkers, E.H., and Helgeson, H.C. (1992) SUPCRT92; a software package for calculating the standard molal thermodynamic properties of minerals, gases, aqueous species, and reactions from 1 to 5000 bar and 0 to 1000 °C. Computers and Geosciences, 18, 899–947.
Kielland, J. (1937) Individual activity coefficients of ions in aqueous solutions. Journal of American Chemical Society, 59, 1675–1678.
Koplitz, L.V., McClure, D.S., and Crerar, D.A. (1987) Spectroscopic study of chloroiron(II) complexes in LiCl-DCl-D_2O solutions. Inorganic Chemistry, 26, 308–313.
Liu, W., McPhail, D.C., and Brugger, J. (2001) An experimental study of copper(I)-chloride and copper(I)-acetate complexing in hydrothermal solutions between 50 °C and 250 °C and vapor-saturated pressure. Geochimica et Cosmochimica Acta, 65, 2937–2948.
Liu, W., Brugger, J., McPhail, D.C., and Spiccia, L. (2002) A spectrophotometric study of aqueous copper(I)-chloride complexes in LiCl solutions between 100 °C and 250 °C. Geochimica et Cosmochimica Acta, 66, 3615–3633.
Liu, W., Etschmann, B., Brugger, J., Foran, G., Spiccia, L., and McInnes, B. (2006) UV-Vis spectrophotometric and XAFS studies of ferric chloride complexes in hyper-saline LiCl solutions at 25–90 °C. Chemical Geology, 231, 326–349.
Mavrogenes, J.A., Berry, A.J., Newville, M., and Sutton, S.R. (2002) Copper speciation in vapor-phase fluid inclusions from the Mole Granite, Australia. American Mineralogist, 87, 1360–1364.
Mayanovic, R.A., Anderson, A.J., Bassett, W.A., and Chou, I.M. (1999) XAFS measurements on zinc chloride aqueous solutions from ambient to supercritical conditions using the diamond anvil cell. Journal of Synchrotron Radiation, 6, 195–197.
Newville, M., Livins, P., Yacoby, Y., Rehr, J.J., and Stern, E.A. (1993) An Improved Background Removal Method for XAFS. Japanese Journal of Applied Physics Part 1-Regular Papers Short Notes and Review Papers, 32, 125–127.
O'Day, P.A., Rivera, N., Root, R., and Carroll, S.A. (2004) X-ray absorption spectroscopic study of Fe reference compounds for the analysis of natural sediments. American Mineralogist, 89, 572–585.
Oelkers, E.H. and Helgeson, H.C. (1991) Calculation of activity coefficients and degrees of formation of neutral ion pairs in supercritical electrolyte solutions. Geochimica et Cosmochimica Acta, 55, 1235–1251.
Ohmoto, H., Hayashi, K.-I., and Kajisa, Y. (1994) Experimental study of the solubilities of pyrite in NaCl-bearing aqueous solutions at 250–350 °C. Geochimica et Cosmochimica Acta, 58, 2169–2185.
Palmer, D.A. and Hyde, K.E. (1993) An experimental determination of ferrous chloride and acetate complexation in aqueous solutions to 300 °C. Geochimica et Cosmochimica Acta, 57, 1393–1408.
Po, H.N. and Sutin, N. (1968) The stability of the monochloro complex of iron(II). Inorganic Chemistry, 7, 621–624.
Pokrovski, G.S., Roux, J., Hazemann, J.L., and Testemale, D. (2005) An X-ray absorption spectroscopy study of argutite solubility and aqueous Ge(IV) speciation in hydrothermal fluids to 500 °C and 400 bar. Chemical Geology, 217, 127–145.
Ruaya, J.R. and Seward, T.M. (1986) The stability of chlorozinc(II) complexes in hydrothermal solutions up to 350 °C. Geochimica et Cosmochimica Acta, 50, 651–661.
Seward, T.M., Henderson, C.M.B., Charnock, J.M., and Driesner, T. (1999) An EXAFS study of solvation and ion pairing in aqueous strontium solutions to 300 °C. Geochimica et Cosmochimica Acta, 63, 2409–2418.
Shock, E.L., Sassani, D.C., Willis, M., and Sverjensky, D.A. (1997) Inorganic species in geologic fluids; correlations among standard molal thermodynamic properties of aqueous ions and hydroxide complexes. Geochimica et Cosmochimica Acta, 61, 907–950.
Simonet, V., Calzavara, Y., Hazemann, J.L., Argoud, R., Geaymond, O., and Raoux, D. (2002) Structure of aqueous $ZnBr_2$ solution probed by X-ray absorption spectroscopy in normal and hydrothermal conditions. Journal of Chemical Physics, 116, 2997–3006.
Susak, N.J. and Crerar, D.A. (1985) Spectra and coordination changes of transition metals in hydrothermal solutions; implications for ore genesis. Geochimica et Cosmochimica Acta, 49, 555–564.
Testemale, D., Argoud, R., Geaymond, O., and Hazemann, J.L. (2005) High pressure, high temperature cell for X-ray absorption and scattering techniques. Review of Scientific Instruments, 76, 043905.
Uchida, E., Naito, M., and Ueda, S. (1998) Aqueous speciation of zinc chloride in supercritical hydrothermal solutions from 500 to 700 °C and 0.5 to 1.0 Kb. Geochemical Journal, 32, 1–9.
van der Lee, J. and De Windt, L. (2001) Present state and future directions of modeling of geochemistry in hydrogeological systems. Contaminant Hydrology, 47, 265–282.
Vinokurov, I.A. and Kankare, J. (1998) Beer's law and the isosbestic points in the absorption spectra of conductive polymers. Journal of Physical Chemistry B, 102, 1136–1140.
Waychunas, G.A., Apted, M.J., and Brown, G.E. Jr. (1983) X-Ray *K*-edge absorption spectra of Fe minerals and model compounds: Near-edge structure. Physics and Chemistry of Minerals, 10, 1–9.
Wesolowski, D.J., Benezeth, P., and Palmer, D.A. (1998) ZnO solubility and Zn^{2+} complexation by chloride and sulfate in acidic solutions to 290 °C with in-situ pH measurement. Geochimica et Cosmochimica Acta, 62, 971–984.
Westre, T.E., Kennepohl, P., DeWitt, J.G., Hedman, B., Hodgson, K.O., and Solomon, E.I. (1997) A multiplet analysis of Fe *K*-edge $1s \rightarrow 3d$ pre-edge features of iron complexes. Journal of the American Chemical Society, 119, 6297–6314.
Wilke, M., Farges, F., Petit, P.E., Brown, G.E., and Martin, F. (2001) Oxidation state and coordination of Fe in minerals: An Fe *K*-XANES spectroscopic study. American Mineralogist, 86, 714–730.
Wood, S.A., Crerar, D.A., and Borcsik, M.P. (1987) Solubility of the assemblage pyrite-pyrrhotite-magnetite-sphalerite-galena-gold-stibnite-bismuthinite-argentite-molybdenite in H_2O-NaCl-CO_2 solutions from 200 °C to 350 °C. Economic Geology 82, 1864–1887.
Zhao, R.H. and Pan, P.J. (2001) A spectrophotometric study of Fe(II)-chloride complexes in aqueous solutions from 10 to 100 °C. Canadian Journal of Chemistry-Revue Canadienne De Chimie, 79, 131–144.

Manuscript received February 2, 2006
Manuscript accepted November 30, 2006
Manuscript handled by David Cole